

Article

Plasma-Assisted Selective Catalytic Reduction for Low-Temperature Removal of NO_x and Soot Simulant

Van Toan Nguyen ¹, Duc Ba Nguyen ^{1,2} , Iljeong Heo ³ and Young Sun Mok ^{1,*} 

¹ Department of Chemical and Biological Engineering, Jeju National University, Jeju 63243, Korea; bkqs2020@gmail.com (V.T.N.); band@plasma.ac.vn (D.B.N.)

² Center for Advanced Chemistry, Institute of Research and Development, Duy Tan University, 03 Quang Trung, Da Nang 550000, Vietnam

³ Environment & Sustainable Resources Research Center, Korea Research Institute of Chemical Technology, Daejeon 34114, Korea; zaiseok@kRICT.re.kr

* Correspondence: smokie@jejunu.ac.kr; Tel.: +82-64-754-3682; Fax: +82-64-755-3670

Received: 8 September 2019; Accepted: 11 October 2019; Published: 13 October 2019



Abstract: The challenge that needs to be overcome regarding the removal of nitrogen oxides (NO_x) and soot from exhaust gases is the low activity of the selective catalytic reduction of NO_x at temperatures fluctuating from 150 to 350 °C. The primary goal of this work was to enhance the conversion of NO_x and soot simulant by employing a Ag/α-Al₂O₃ catalyst coupled with dielectric barrier discharge plasma. The results demonstrated that the use of a plasma-catalyst process at low operating temperatures increased the removal of both NO_x and naphthalene (soot simulant). Moreover, the soot simulant functioned as a reducing agent for NO_x removal, but with low NO_x conversion. The high efficiency of NO_x removal required the addition of hydrocarbon fuel. In summary, the combined use of the catalyst and plasma (specific input energy, SIE ≥ 60 J/L) solved the poor removal of NO_x and soot at low operating temperatures or during temperature fluctuations in the range of 150–350 °C. Specifically, highly efficient naphthalene removal was achieved with low-temperature adsorption on the catalyst followed by the complete decomposition by the plasma-catalyst at 350 °C and SIE of 90 J/L.

Keywords: removal of NO_x and soot; plasma-catalyst; DBD; low-temperature; non-thermal plasma

1. Introduction

There is considerable attention being paid to the removal of nitrogen oxides (NO_x) and soot produced by diesel engines [1–6], because these engines using petroleum products continue to be a crucial energy source [7]. However, the emission of CO, hydrocarbons (HCs), NO_x, and soot (particulate matter) from diesel engines is an environmental concern, because these gases are a major source of air pollution [8]. The instantaneous substitution of diesel engines with environmentally friendly systems, namely wind power plants, solar power plants, and electric cars would have considerable economic consequences. Moreover, diesel-powered equipment is noted for its high energy efficiency along with low CO₂ emission. Therefore, the reduction of harmful emissions from diesel engines constitutes an effective way of addressing these problems. Nowadays, sustainable development is becoming increasingly crucial and consequently, stricter legislation has been introduced to reduce harmful gas emissions [7], e.g., Euro 6 for gas emission by cars and light trucks in the European Union from September 2014 [9]. Therefore, the reduced emission of harmful gases is required to achieve standard emission regulations. The removal of harmful gases, such as NO_x and soot, from exhaust gases before it is released to the atmosphere would be an effective method in this regard.

During the last three decades, many researchers have devoted their efforts to the removal of NO_x and soot generated by diesel engines by employing catalysts [10–17]. The two most common ways of accomplishing this are selective catalytic reduction (SCR) and NO_x storage-reduction (NSR) based on NO_x adsorbers [18–22]. The SCR and NSR can be combined with catalytic diesel particulate filters (DPF) for simultaneous removal of NO_x and soot. The catalytic DPF and their regeneration by means of microwaves have been reported in the literature [23–25]. Both of these approaches involve a reduction step that requires high temperatures to obtain high-efficiency removal of NO_x and soot [26–33]. Unfortunately, in many specific cases, the sources of NO_x and soot emission have a temperature lower than the activation temperature of the catalyst. Therefore, results have either shown the effectiveness of the catalyst to be low at that temperature or that it is necessary to heat the system, suggesting a decrease in economic efficiency. Thus, the removal of NO_x and soot at a low temperature is a worthy research topic that remains of interest to enhance the economic efficiency and to facilitate practical application [34–38].

SCR, such as with Ag/Al₂O₃, is appropriate for NO_x removal because of the low cost of Ag in comparison with other noble metals, suggesting a high practical application potential [14,37]. The activity of the catalyst sharply decreases at low operating temperatures (<300 °C), owing to the narrow active temperature window (300–350 °C) for NO_x removal [39,40]. Unfortunately, the soot in the gas exhausted by diesel engines consists of heavy hydrocarbons that are emitted to the atmosphere as solid particles due to the incomplete burning of diesel fuels [41]. This suggests that low temperatures do not facilitate the removal of NO_x and soot. In this respect, advances in plasma techniques, such as dielectric barrier discharge (DBD), hold advantages because they generate a cocktail of reactive chemical species such as electrons, radicals, and excited gas molecules and ions, at low temperature. In the catalyst or plasma-catalyst process, the heavy hydrocarbon undergoes partial oxidization to other derivative hydrocarbons, such as aldehydes, which have low-temperature activity for NO_x removal. By the presence of the reactive chemical cocktails in the case of plasma coupled with a catalyst, an increase in the oxidation of the original heavy hydrocarbons to aldehyde compounds is expected [42–46]. Notably, there is poor NO_x removal with the plasma-catalyst process in the case of the absence of reducing agents such as hydrocarbons, mainly oxidation NO to NO₂. Plasma coupled with a catalyst, therefore, enables the removal of both NO_x and soot at low operating temperatures. Moreover, enhanced NO_x removal under fluctuating temperatures was also observed in the presence of plasma [47–50].

In this study, the use of HC-SCR for the removal of NO_x and soot simulatant was investigated by combining a Ag/α-Al₂O₃ catalyst with a DBD reactor and by varying the specific input energy (SIE) and temperature. Simulated diesel exhaust gas was obtained by preparing a mixture of 300 ppm NO, 265 ppm n-heptane (C₇H₁₆), 48 ppm naphthalene as a soot simulatant, 3.7% water vapor, 10% O₂, with the balance consisting of N₂. The removal of NO_x and naphthalene was examined in the operating temperature range from 150 to 350 °C and by varying the SIE in the range up to 210 J/L. The result indicated that the presence of plasma enhanced the efficiency of removing NO_x and soot simulatant at low temperatures. In addition, the presence of n-heptane in the feed promoted both NO_x and soot simulatant removal. The role of plasma to achieve the removal of NO_x and soot simulatant under fluctuating operating temperatures was also examined and is discussed.

2. Results

2.1. Effects of Plasma input Parameters on Discharge Power

Figure 1 indicates an increase in discharge power as a function of the temperature and applied voltage. According to the Lissajous figure method [51], the deposition of the input energy of the DBD system depends on the applied voltage and electrical charge of DBD. Consequently, high-amplitude voltage led to a considerable discharge power. The discharge power also increased at high temperatures, which can be explained by an increase in the DBD charge. Indeed, the discharge power can be estimated by the area of voltage-charge figures. When the amplitude of the voltage was maintained while

increasing the operating temperature, the amount of charge increased and, in turn, the area of the voltage-charge figure, as well as the discharge power, became large [49].

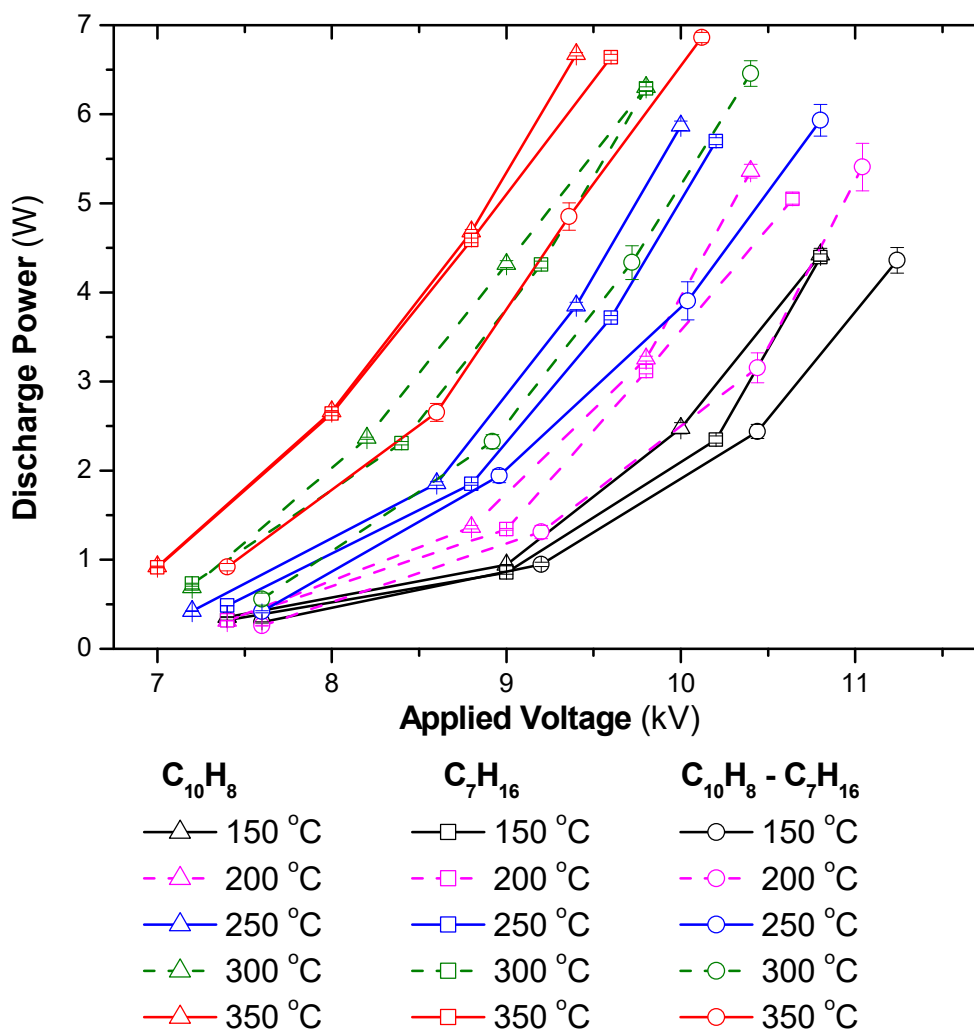


Figure 1. Discharge power as a function of temperature and applied voltage for different gas compositions (total flow rate fixed at 2 L/min including 3.7% H₂O, 10% O₂, reducing agents: 48 ppm C₁₀H₈, 265 ppm C₇H₁₆, N₂ as balance; acquire mode of the oscilloscope: average of 128 waveforms).

This figure also demonstrates that the presence of n-heptane and naphthalene at a level of a few hundred ppm could change the discharge power significantly. This phenomenon was also observed when the CHF₃ concentration was changed to a few thousand ppm in the feed in the DBD discharge [52]. Equation (1), which is adapted from published work [53–55], can be used to estimate the discharge power that is suitable for the plasma-catalyst system and the sinusoidal voltage waveform in this experiment. As understood from Equation (1), the inclusion of n-heptane and naphthalene in the feed can significantly change R and C_{cg}, due to the changes in the gas composition and the surface properties of the catalyst when adsorbing the reactants. Moreover, the resistance and capacitance of the materials strongly depend on the temperature. In summary, the discharge power strongly depends on the applied voltage and the temperature of the plasma system. The dependence of the discharge power on the gas composition in the feed followed the order (C₁₀H₈ + C₇H₁₆) < C₇H₁₆ < C₁₀H₈, which was correlated with the concentration of CO₂ produced during the experiments, i.e., the CO₂ produced

was in the order: $C_{10}H_8 < C_7H_{16} < (C_{10}H_8 + C_7H_{16})$. This suggests that the discharge power tended to decrease as the concentration of CO_2 in the discharge zone increased.

$$P = \frac{V_{DBD}^2}{2} \frac{1}{R(1 + \frac{C_{cg}}{C_d})^2 + \frac{1}{\omega^2 C_d^2 R}} \quad (1)$$

where

V_{DBD} is the amplitude of the voltage applied to the reactor

R is the equivalent resistance of the reactor system

C_{cg} is the equivalent capacitance of the catalyst and gas gap

C_d is the absolute capacitance of the dielectric layers.

2.2. Removal of NO_x and Soot Simulant by SCR Coupled with Plasma

Naphthalene (soot simulant) played the role of the reducing agent in the SCR of NO_x as shown in Figure 2a. The conversion of NO_x was 8 to 20% in the temperature range of 200–350 °C along with SIE of 0–210 J/L. The SIE is defined as the power in W divided by gas flow rate in L/s. The removal of NO_x tended to increase with the increasing temperature and SIE. The previous reports indicated that without a reducing agent, NO_x removal neither occurred in the plasma nor in the plasma-catalyst processes, only in the oxidization of NO to NO_2 [42,50]. Naphthalene containing two aromatic rings can function as a reducing agent [27,56]. Similar to other hydrocarbons, naphthalene produces partially oxidized intermediate products. Subsequently, NO_x reduction is performed via the chemical reactions with the intermediate products. For this experiment, the concentration of naphthalene was 48 ppm. It is argued that this low concentration is the reason for the low NO_x removal. Figure 2b shows the concentration of NO and NO_2 when the temperature varies from 200 to 300 °C and SIE varies from 0 to 210 J/L. This demonstrated that a part of NO was oxidized to NO_2 in the presence of plasma. The catalytic destruction of naphthalene hardly occurs at low temperatures because it is stabilized by resonance hybrid, i.e., high temperature and high SIE are needed for the decomposition of this compound. Figure 2c indicates that, even at an operating temperature of 350 °C, naphthalene conversion was approximately 40%. However, almost all naphthalene was destroyed with SIE above 90 J/L in the temperature range of 200–350 °C. Furthermore, the selectivity toward CO_2 increased as the temperature and SIE increased, as shown in Figure 2d. Overall, the soot simulant (naphthalene) can function as a reducing agent of SCR for NO_x removal. Further, poor catalytic destruction of naphthalene at low temperatures can be overcome with the help of plasma.

According to the above results, the soot simulant can act as a reducing agent for SCR of NO_x . However, the efficiency of NO_x removal was not satisfactory with 48 ppm naphthalene tantamount to a C/N ratio of 1.6 (the ratio of carbon concentration in the hydrocarbon to nitrogen concentration in NO_x). Previous reports indicated that n-alkane is an effective reducing agent for the HC-SCR process [48–50]. In general, dodecane ($C_{12}H_{26}$) can represent diesel fuel. However, this component has low vapor pressure, making it difficult to vaporize and inject to the feed gas. Thus, for the simplicity of the experimental procedure, n-heptane having relatively low vapor pressure was used as a reducing agent instead of dodecane. The effect of n-heptane on the simultaneous removal of NO_x and the soot simulant was examined at temperatures ranging from 200 to 350 °C and SIE from 0 to 210 J/L. The results are shown in Figure 3.

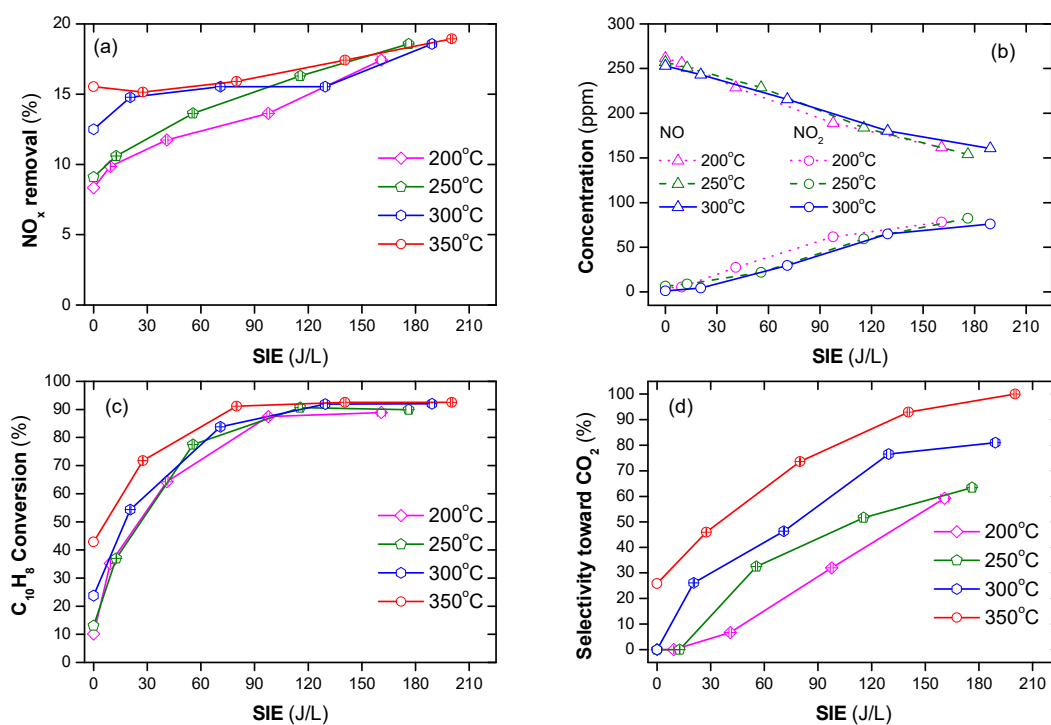


Figure 2. NO_x and naphthalene removal by plasma-catalyst at various temperatures and specific input energy (SIE) (a) NO_x conversion, (b) concentrations of NO and NO₂, (c) naphthalene conversion, and (d) selectivity toward CO₂ (total flow rate of 2 L/min including: 300 ppm NO, 48 ppm naphthalene, 3.7% H₂O, 10% O₂, and N₂ as balance).

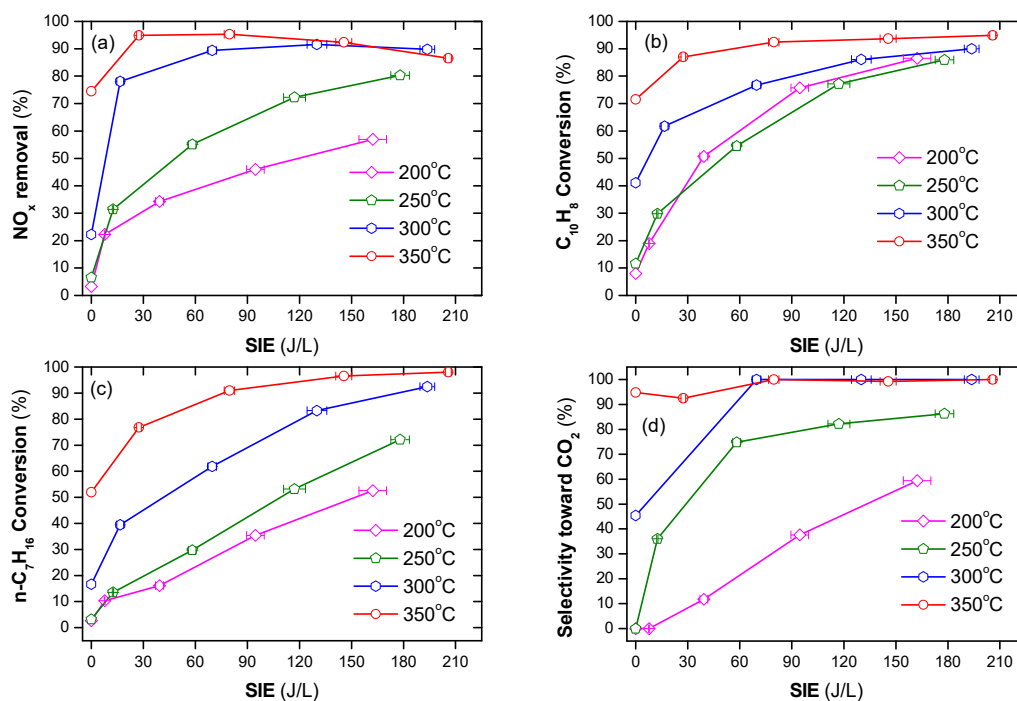


Figure 3. NO_x and naphthalene removal by plasma-catalyst at various temperatures and SIE values (a) NO_x conversion, (b) naphthalene conversion, (c) n-heptane conversion, and (d) selectivity toward CO₂ (total flow rate of 2 L/min including: 300 ppm NO, 48 ppm naphthalene, 265 ppm n-heptane, 3.7% H₂O, 10% O₂, and N₂ as balance).

The efficiency of NO_x removal increased sharply when a combination of plasma and n-heptane was used, as shown in Figure 3a,b. Specifically, at an operating temperature at or below $250\text{ }^\circ\text{C}$, the presence of only n-heptane did not remove NO_x and naphthalene. On the other hand, increasing the SIE value increased the removal of NO_x and naphthalene. At an operating temperature of $300\text{ }^\circ\text{C}$, NO_x removal without plasma was approximately 22%, whereas a sharp increase was observed in the presence of plasma. The conversion of naphthalene also largely increased to 62–90%, depending on the SIE value. The efficiency of both NO_x and soot simulant removal increased in the presence of n-heptane at $350\text{ }^\circ\text{C}$ or across the entire temperature range when coupled with plasma. Figure 3c demonstrates that there is a correlation between the increase in NO_x removal and n-heptane conversion. This also suggests that n-heptane is the main reducing agent for the NO_x removal process. The tendency of CO_2 to be produced from n-heptane as well as naphthalene increasing with the operating temperature and SIE, is shown in Figure 3d. This indicates that, at a high temperature and input energy, complete oxidization of n-heptane and naphthalene to CO_2 occurred, i.e., the selectivity toward CO_2 , is nearly 100% at $350\text{ }^\circ\text{C}$ and $\text{SIE} \geq 80\text{ J/L}$.

The presence of n-heptane, at operating temperatures at or above $300\text{ }^\circ\text{C}$ or the presence of plasma at low temperatures, can account for the increase in NO_x and naphthalene removal. This is in line with the previous report [50], which indicated that the conversion of n-heptane to derivative hydrocarbons or CO_2 started to occur at $290\text{ }^\circ\text{C}$ over the $\text{Ag}/\alpha\text{-Al}_2\text{O}_3$ catalyst, whereas the plasma-catalyst process induced n-heptane conversion at a low operating temperature. Consequently, with the catalyst alone, n-heptane neither enhanced the removal of NO_x nor that of naphthalene at a low operating temperature ($\leq 250\text{ }^\circ\text{C}$), as shown in Figure 4. The conversion of NO_x and n-heptane by the catalytic process decreased in the presence of naphthalene. These phenomena are caused by the adsorption of naphthalene on the catalyst, which deactivates the catalytic active sites. However, the issue was solved by using plasma. Consequently, at high SIE ($\geq 90\text{ J/L}$) and operating temperatures at or above $300\text{ }^\circ\text{C}$, more than 70% of NO_x , naphthalene, and n-heptane were converted.

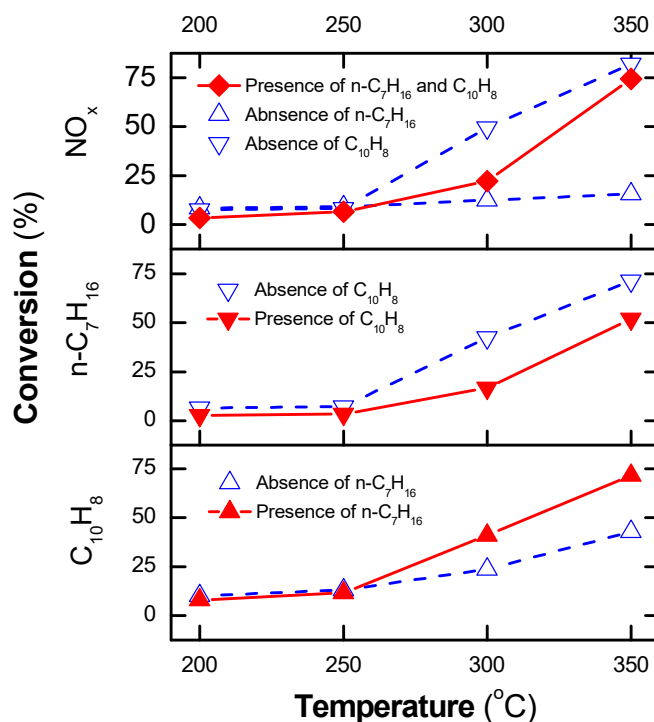


Figure 4. NO_x conversion and conversion of n-heptane and naphthalene by catalytic process with/out n-heptane and naphthalene at various operating temperatures (total flow rate fixed at 2 L/min, including 300 ppm NO , 48 ppm naphthalene, 265 ppm n-heptane, 3.7% H_2O , 10% O_2 , and N_2 as balance).

Figure 5 demonstrates the difference between using 48 ppm naphthalene (C/N = 1.6) and 265 ppm n-heptane (C/N = 6) as a reducing agent during the NO_x removal process at an operating temperature of 250 °C. A larger amount of NO is converted or oxidized to NO₂ when n-heptane is present in the feed gas. However, the presence of naphthalene presented little conversion or oxidization of NO. Regarding the mechanism during NO_x removal by the plasma-catalyst (R1–R6), NO can be oxidized to NO₂, which is allowable according to R1–R2. In fact, in the absence of hydrocarbon, NO_x was not removed by using the plasma-catalyst process. However, in the presence of hydrocarbon in conjugation with plasma, NO_x removal can be performed by other reactions (R3–R6), which are also adapted from the same paper [50]. The difference between n-heptane and naphthalene during the NO_x removal process can be explained by the differences in the molecular structure (naphthalene: polycyclic aromatic hydrocarbon; n-heptane: straight-chain hydrocarbons) and in the bond dissociation energies (BDEs) of C-H and C-C in naphthalene and n-heptane. For information, the BDEs of C-H and C-C in n-heptane are (410–415.7 kJ/mol) and (361.0–368.2 kJ/mol), respectively, whereas those of naphthalene are (469.4–482.8 kJ/mol) [57]. Another reason was that the total carbon concentration in 265 ppm n-heptane (1855 ppm carbon) was higher than that of 48 ppm naphthalene (480 ppm carbon).

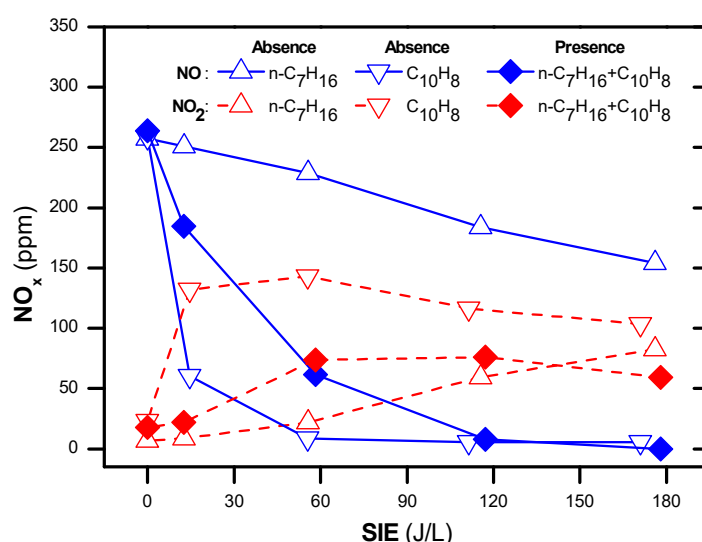
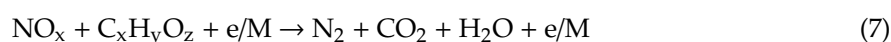
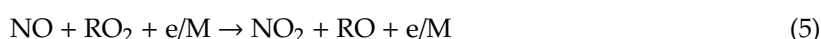
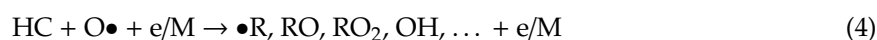


Figure 5. Concentrations of NO and NO₂ as a function of SIE for different gas compositions at 250 °C (total flow rate of 2 L/min including: 300 ppm NO, 265 ppm n-heptane, 48 ppm naphthalene, 3.7% H₂O, 10% O₂ and N₂ as balance).



Here, *e* denotes energetic electrons, and *M* stands for excited molecules.

2.3. Removal of NO_x and Soot Simulant during Operating Temperature Fluctuations

The temperature of the exhaust gas ordinarily fluctuates and depends on the operating state, e.g., the gas temperature of diesel-powered passenger cars fluctuates in the range of 180–350 °C [58]. This suggests that the performance of NO_x and soot removal over a catalyst subjected to a temperature fluctuation is a factor when evaluating the catalyst for potential practical applications. This section discusses the removal of NO_x and the soot simulant by increasing the temperature at a rate of 3 °C/min in the range of 150–350 °C and by increasing the average SIE within the first 70 min from 0 to 177 J/L.

The catalyst temperature window was expanded by the presence of plasma, as shown in Figure 6. As seen, the catalyst-alone process reduced the concentration of NO_x effectively when the operating temperature was above 300 °C. On the contrary, the plasma catalyst can obtain a low concentration of NO_x at operating temperatures from 150 °C upward. The concentration of NO_x decreased with increasing SIE_{avg}. However, at a high temperature (≥ 300 °C) and high SIE (177 J/L), the NO_x concentration increased slightly due to the generation of NO_x by plasma, as shown in Figure 6a. As indicated by the above result, the discharge power depends on the discharge state, i.e., the temperature, applied voltage, and gas composition. Therefore, during a temperature fluctuation, the discharge power necessarily changed with the processing time. As seen in Figure 6b, the discharge power increased with the operating temperature. The average SIE, i.e., SIE_{avg}, can be estimated using Equation (8), and the average NO_x removal using Equation (9). As a result, the average NO_x removal within the first 70 min as a function of average of SIE was plotted as shown in Figure 6c. This suggests that poor NO_x removal under the conditions of a temperature fluctuation during the catalytic process can be improved by the combination of plasma with an average SIE of 60–120 J/L.

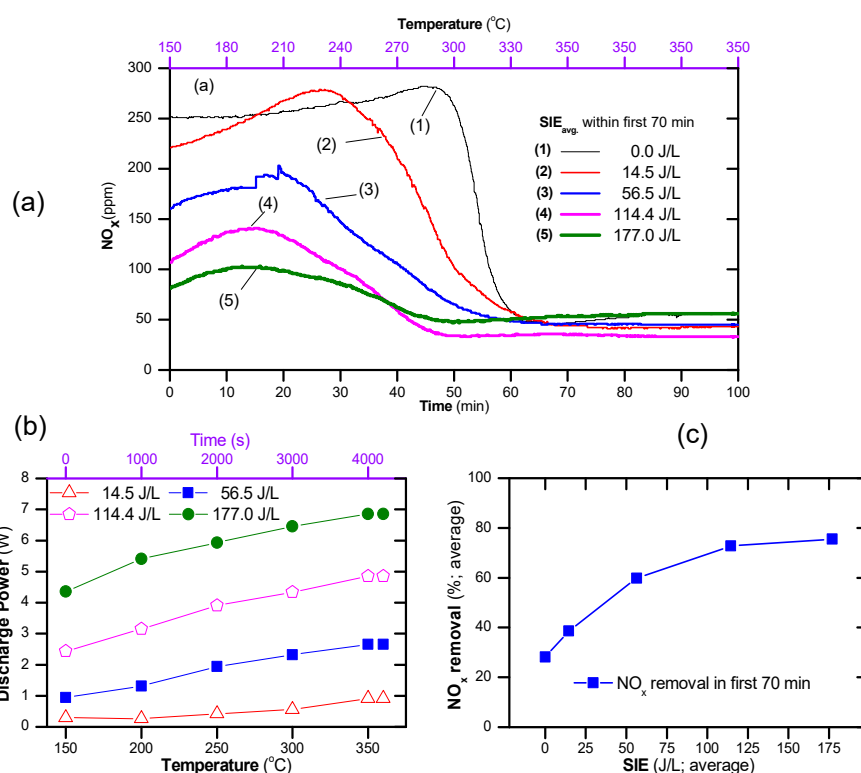


Figure 6. (a) Evolution of NO and NO₂ during the temperature increase from 150 to 350 °C at a rate of 3 °C/min and then being maintained at 350 °C for both catalyst and plasma-catalyst, (b) changes in discharge power with temperature, and (c) average NO_x conversion in the first 70 min (total flow rate of 2 L/min including: 300 ppm NO, 48 ppm naphthalene, 265 ppm n-heptane 3.7% H₂O, 10% O₂ and N₂ as balance; the catalyst was exposed to the feed gas for 15 min at 150 °C before starting the temperature increase).

$$SIE_{avg} = \frac{1}{(t_2 - t_1) \times F} \int_{t_1}^{t_2} P(t) dt \quad (8)$$

$$Conversion_{avg} = 1 - \frac{1}{(t_2 - t_1)} \int_{t_1}^{t_2} \left(\frac{C}{C_0} \right) dt \quad (9)$$

Here, F denotes total flow rate, $[t_1 - t_2]$ is the time duration for collecting data during temperature fluctuation, and the subscript “avg” indicates the average value.

The ratio of the concentration at the outlet and inlet (C/C_0) for both naphthalene and n-heptane during the temperature program (150–350 °C at a rate of 3 °C/min) is shown in Figure 7. The initial increases of naphthalene at low SIE_{avg} can be explained by the desorption. Due to its low vapor pressure, naphthalene adsorbed at low temperatures, after which it underwent desorption at high operating temperatures. Here, the temperature at which C/C_0 of naphthalene reached a maximum value decreased as the SIE increased. This is a result of the decomposition of naphthalene by plasma. Specifically, the temperature showing the maximum for the catalyst-alone process was 315 °C, whereas the temperatures showing the maximum decreased to 270 and 250 °C with SIE_{avg} of 14.5 and 56.5 J/L, respectively. Not only the temperatures showing the maximum, but also C/C_0 of naphthalene largely decreased with the combination of plasma. In the case of high SIE_{avg} of 114.4 and 177.0 J/L, almost all naphthalene in the feed was removed. In contrast to naphthalene, the concentration of n-heptane did not show the maximum, and decreased as the SIE and operating temperature increased. The difference between n-heptane and naphthalene is due to their adsorption capabilities and vapor pressures. Note that the vapor pressure of n-heptane (3985 Pa at 290 K) is greater than that of naphthalene (4.9 Pa at 290 K). In summary, the presence of plasma enhanced the removal of NO_x and naphthalene under fluctuating temperature conditions.

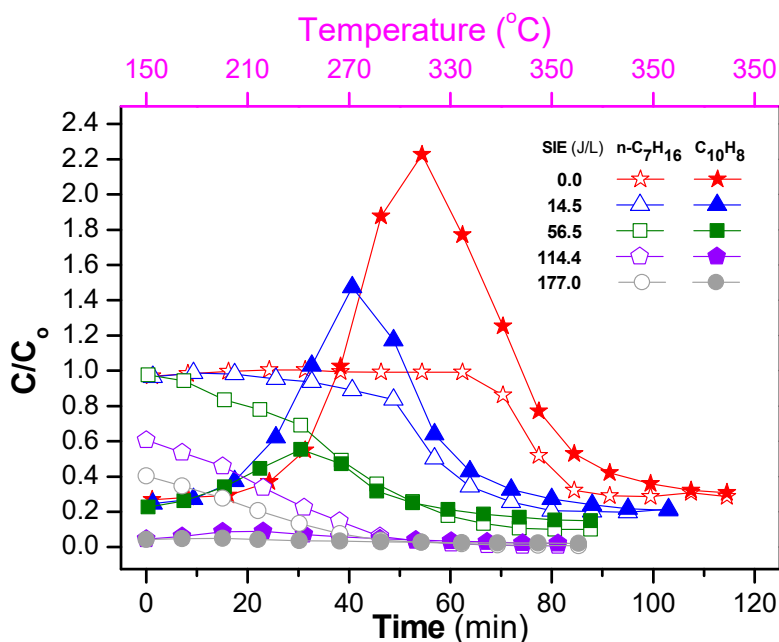


Figure 7. Evolution of concentration ratio of outlet and inlet (C/C_0) of naphthalene and n-heptane during the temperature increase from 150 to 350 °C with a rate of 3 °C/min and then being maintained at 350 °C for both catalyst and plasma-catalyst (the conditions are the same as in Figure 6).

3. Materials and Methods

3.1. Preparation of Ag/ α -Al₂O₃ Catalyst

The DBD plasma reactor was charged with a 20 g Ag/ α -Al₂O₃ (Ag: 2 wt%) catalyst and used for the SCR of NO_x and soot simulant removal. The preparation of Ag/ α -Al₂O₃ is described elsewhere [49]. Briefly, the catalyst was synthesized by the incipient wetness impregnation method, i.e., α -Al₂O₃ pellets (3 mm, 30 g; 414,069 Sigma-Aldrich, St. Louis, MO, USA) were impregnated with an aqueous solution of 0.966 g AgNO₃ (12 mL; Assay 99.8%, Daejung, Korea). Subsequently, the impregnated pellets were exposed to the atmosphere for 3 h, and then dried overnight at 110 °C and calcined for 6 h at 550 °C.

3.2. Plasma Coupled with SCR for NO_x and Soot Simulant Removal

A schematic diagram of the experimental setup is shown in Figure 8. The Ag/ α -Al₂O₃ catalyst (20 g) was placed in the reactor tube (25.17 mL) using a packing length of 65 mm. The volume was created by a threaded rod (power electrode) with a diameter of 6 mm located at the center of the alumina tube (ID = 23 mm, OD = 29 mm). The position of the power electrode, as well as the catalyst, was fixed by two porous ceramic rings. The copper foil (length = 75 mm) was wrapped around the alumina tube as a grounded electrode. The total flow rate was fixed at 2 L/min; therefore, the hourly space velocity of the gas was 4768 h⁻¹. The feed gas, which comprised a mixture of 300 ppm NO, 48 ppm naphthalene, 265 ppm n-heptane, 10% O₂, 3.7% H₂O, and N₂ as the balance, was delivered to the reaction zone by mass flow rate controllers (AFC500, Atovac Co., Yongin, Korea). Herein, the concentration of naphthalene was maintained by passing a mixture of O₂ and N₂ through an Erlenmeyer flask containing naphthalene powder. The flask was kept in a water bath at 17 °C. Subsequently, the flow passed through the saturated aqueous solution of naphthalene. Pure water was used when naphthalene was absent from the feed. The concentration of n-heptane was varied by allowing 15 mL/min of N₂ to flow through an Erlenmeyer flask containing n-heptane, and the temperature was maintained at 15 °C by using a water bath. Then, 300 ppm of NO was introduced to the feed gas. However, because NO was spontaneously oxidized to NO₂ during the gas mixing process, the feed gas contained 285 NO and 15 ppm NO₂ after the mixture was prepared.

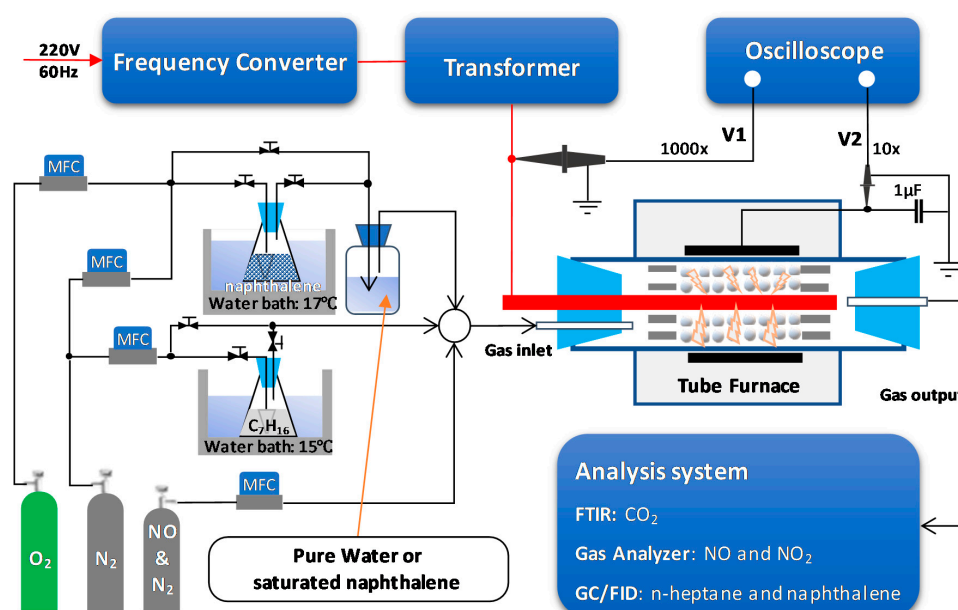


Figure 8. Schematic diagram of the experimental setup for removal of NO_x and soot.

Atmospheric pressure plasma was generated by using 400 Hz sinusoidal voltage, which was supplied by a frequency converter (Sampoong Power Co., Ltd., Incheon, Korea) and integrated with a transformer (Taehwa Electric Co., Seoul, Korea). During the plasma-catalytic reactions, electrical waveforms were monitored and recorded by a digital oscilloscope (TBS1064, 60MHz with 4 channels, Tektronix, Beaverton, OR, USA), in which the applied voltage (V_1) was measured with a high-voltage probe (P6015A, Beaverton, OR, USA), while a low-voltage probe (P6139B for, Beaverton, OR, USA) was used to measure the voltage across the 1 μ F capacitor (V_2). The discharge power was estimated by the Lissajous figure method (Equation (10)). The concentrations of NO_x and CO_2 were measured by a gas analyzer (rbr-ecom-KD, rbr-Computertechnik GmbH, Iserlohn, Germany) and a Fourier transform infrared spectrophotometer (FTIR-7600, Lambda Scientific, Australia), respectively. The concentrations of naphthalene and n-heptane were measured with a gas chromatograph (GC, DS6200, DS Science Inc., Seoul, Korea). The GC was equipped with a 60-m long capillary column (DS-624, DS Science Inc., Seoul, Korea) and a flame ionization detector (FID) in order to separate and detect naphthalene and n-heptane in the outlet gas. The analysis was conducted by defining several terms as below.

$$\text{Discharge power, } P(W) = f \int_{t_0 - \frac{T}{2}}^{t_0 + \frac{T}{2}} V_{DBD}(t) dq(t) = f C \sum_{k=1}^n \left(\frac{V_{1k+1} - V_{2k+1} + V_{1k} - V_{2k}}{2} \right) (V_{2k+1} - V_{2k}) \quad (10)$$

$$\text{Specific input energy, } SIE \left(\frac{J}{L} \right) = \frac{P \left(\frac{J}{s} \right)}{F \left(\frac{L}{s} \right)} \quad (11)$$

$$[\text{NO}_x] = [\text{NO}] + [\text{NO}_2] \quad (12)$$

$$\text{NO}_x \text{ removal, } Conv.\text{NO}_x (\%) = \left(1 - \frac{C_{\text{NO}_x}^{\text{outlet}}}{C_{\text{NO}_x}^{\text{in feed}}} \right) \times 100\% \quad (13)$$

$$\text{Selectivity toward CO}_2, S_{\text{CO}_2} (\%) = \frac{C_{\text{CO}_2}^{\text{outlet}}}{7(C_{\text{n-heptane}}^{\text{inlet}} - C_{\text{n-heptane}}^{\text{outlet}}) + 10(C_{\text{naphthalene}}^{\text{inlet}} - C_{\text{naphthalene}}^{\text{outlet}})} \times 100\% \quad (14)$$

4. Conclusions

This research aimed to examine the removal of NO_x and the soot simulant from diesel emissions in a fixed-bed DBD reactor in the temperature range from 150 to 350 °C. The results presented that the presence/absence of naphthalene (48 ppm) and n-heptane (265 ppm) affected the discharge power of the plasma-catalyst system. The soot simulant and naphthalene can play the role of reducing agents in the NO_x removal process. However, high-efficiency NO_x removal requires an additional reducing agent. The $\text{Ag}/\alpha\text{-Al}_2\text{O}_3$ presented a narrow temperature window for NO_x and soot simulant removal. However, the presence of plasma expanded the temperature window toward low operating temperatures. As a result, the high efficiency of NO_x and soot simulant removal were obtained by using the catalyst coupled with plasma under fluctuating temperature conditions.

Author Contributions: V.T.N. and D.B.N. carried out the experimental work and analyzed the data; I.H. participated in the interpretation of the results; Y.S.M. supervised all the study.

Funding: This work has been performed as a part of Project No. SI1913-20 by the Korea Research Institute of Chemical Technology (KRICT) and No. CAP-18-08-KIMM by the National Research Council of Science & Technology (NST) grant by the Korea government (MSIP).

Conflicts of Interest: The authors declare no conflicts of interest.

References

1. More, P.M. Effect of active component addition and support modification on catalytic activity of Ag/Al₂O₃ for the selective catalytic reduction of NO_x by hydrocarbon—A review. *J. Environ. Manag.* **2017**, *188*, 43–48. [CrossRef]
2. Gao, F.; Tang, X.; Yi, H.; Zhao, S.; Li, C.; Li, J.; Shi, Y.; Meng, X. A review on selective catalytic reduction of NO_x by NH₃ over Mn-based catalysts at low temperatures: Catalysts, mechanisms, kinetics and DFT calculations. *Catalysis* **2017**, *7*, 199. [CrossRef]
3. Xu, J.; Wang, H.; Guo, F.; Zhang, C.; Xie, J. Recent advances in supported molecular sieve catalysts with wide temperature range for selective catalytic reduction of NO_x with C₃H₆. *RSC Adv.* **2019**, *9*, 824–838. [CrossRef]
4. Wang, J.; Zhao, H.; Haller, G.; Li, Y. Recent advances in the selective catalytic reduction of NO_x with NH₃ on Cu-Chabazite catalysts. *Appl. Catal. B Environ.* **2017**, *202*, 346–354. [CrossRef]
5. Zhang, L.; Wu, Q.; Meng, X.; Müller, U.; Feyen, M.; Dai, D.; Maurer, S.; McGuire, R.; Moini, A.; Parvulescu, A.N.; et al. Recent advances in the preparation of zeolites for the selective catalytic reduction of NO_x in diesel engines. *React. Chem. Eng.* **2019**, *4*, 975–985. [CrossRef]
6. Lambert, C.K. Perspective on SCR NO_x control for diesel vehicles. *React. Chem. Eng.* **2019**, *4*, 969–974. [CrossRef]
7. Johnson, T.; Joshi, A. *Review of Vehicle Engine Efficiency and Emissions*; SAE Tech. Paper 2018-01-0329; SAE International: Warrendale, PA, USA, 2018. [CrossRef]
8. Jacobson, M.Z. *Air Pollution and Global Warming: History, Science, and Solutions*; Cambridge University Press: Cambridge, UK, 2012.
9. Emission Standards: European Union: Cars and Light Trucks. Available online: <https://www.dieselnet.com/standards/eu/ld.php#stds> (accessed on 15 April 2019).
10. Tan, J.; Wei, Y.; Sun, Y.; Liu, J.; Zhao, Z.; Song, W.; Li, J.; Zhang, X. Simultaneous removal of NO_x and soot particulates from diesel engine exhaust by 3DOM Fe–Mn oxide catalysts. *J. Ind. Eng. Chem.* **2018**, *63*, 84–94. [CrossRef]
11. Matarrese, R.; Morandi, S.; Castoldi, L.; Villa, P.; Lietti, L. Removal of NO_x and soot over Ce/Zr/K/Me (Me = Fe, Pt, Ru, Au) oxide catalysts. *Appl. Catal. B: Environ.* **2017**, *201*, 318–330. [CrossRef]
12. Tauzia, X.; Maiboom, A.; Karaky, H. Semi-physical models to assess the influence of CI engine calibration parameters on NO_x and soot emissions. *Appl. Energy* **2017**, *208*, 1505–1518. [CrossRef]
13. Wang, L.; Fang, S.; Feng, N.; Wan, H.; Guan, G. Efficient catalytic removal of diesel soot over Mg substituted K/La_{0.8}Ce_{0.2}CoO₃ perovskites with large surface areas. *Chem. Eng. J.* **2016**, *293*, 68–74. [CrossRef]
14. Urán, L.; Gallego, J.; Li, W.Y.; Santamaría, A. Effect of catalyst preparation for the simultaneous removal of soot and NO_x. *Appl. Catal. A Gen.* **2019**, *569*, 157–169. [CrossRef]
15. Mao, L.; Yan, Y.; Zhao, X.; Fu, M.; Xiao, Y.; Dong, G. Comparative study on removal of NO_x and soot with a-site substituted La₂NiO₄ perovskite-like by different valence cation. *Catal. Lett.* **2019**, *149*, 1087–1099. [CrossRef]
16. Yang, L.; Zhang, C.; Shu, X.; Yue, T.; Wang, S.; Deng, Z. The mechanism of Pd, K co-doping on Mg–Al hydrotalcite for simultaneous removal of diesel soot and NO_x in SO₂-containing atmosphere. *Fuel* **2019**, *240*, 244–251. [CrossRef]
17. Zhang, J.; Liu, F.; Liang, J.; Yu, H.; Liu, W.; Wang, X.; Peng, H.; Wu, P. Exploring the nanosize effect of mordenite zeolites on their performance in the removal of NO_x. *Ind. Eng. Chem. Res.* **2019**, *58*, 8625–8635. [CrossRef]
18. Shangguan, W.; Zou, G.; Jiang, Z. Introduction. In *Simultaneous Catalytic Removal of Diesel Soot and NO_x*; Shangguan, W., Zou, G., Jiang, Z., Eds.; Springer: Singapore, 2019; pp. 1–8.
19. Pereda-Ayo, B.; González-Velasco, J.R. NO_x storage and reduction for diesel engine exhaust after treatment. In *Diesel Engine-Combustion, Emissions and Condition Monitoring*; Bari, S., Ed.; InTech: Rijeka, Croatia, 2013.
20. Shangguan, W.; Zou, G.; Jiang, Z. *Simultaneous Catalytic Removal of Diesel Soot and NO_x*; Springer Nature: Singapore, 2019.
21. Shangguan, W.; Zou, G.; Jiang, Z. kinetics study for simultaneous removal of soot and NO_x. In *Simultaneous Catalytic Removal of Diesel Soot and NO_x*; Shangguan, W., Zou, G., Jiang, Z., Eds.; Springer: Singapore, 2019; pp. 71–100.

22. Moliner, M.; Corma, A. From metal-supported oxides to well-defined metal site zeolites: The next generation of passive NO_x adsorbers for low-temperature control of emissions from diesel engines. *React. Chem. Eng.* **2019**, *4*, 223–234. [[CrossRef](#)]
23. Palma, V.; Ciambelli, P.; Meloni, E. Optimising the catalyst load for Microwave susceptible catalysed DPF. *Chem. Eng. Trans.* **2012**, *29*, 637–642.
24. Palma, V.; Ciambelli, P.; Meloni, E.; Sin, A. Optimal CuFe₂O₄ load for MW susceptible catalysed DPF. *Chem. Eng. Trans.* **2013**, *35*, 727–732.
25. Meloni, E.; Palma, V.; Vaiano, V. Optimized microwave susceptible catalytic diesel soot trap. *Fuel* **2017**, *205*, 142–152. [[CrossRef](#)]
26. Xu, J.; Lu, G.; Guo, Y.; Guo, Y.; Gong, X.Q. A highly effective catalyst of Co-CeO₂ for the oxidation of diesel soot: The excellent NO oxidation activity and NO_x storage capacity. *Appl. Catal. A Gen.* **2017**, *535*, 1–8. [[CrossRef](#)]
27. Tsukamoto, Y.; Utaki, S.; Zhang, W.; Fukuma, T.; Kusaka, J. *Effects of Soot Deposition on NO_x Purification Reaction and Mass TRANSFER in a SCR/DPF catalyst*; SAE International: New York, NY, USA, 2018.
28. Borfecchia, E.; Negri, C.; Lomachenko, K.A.; Lamberti, C.; Janssens, T.V.W.; Berlier, G. Temperature-dependent dynamics of NH₃-derived Cu species in the Cu-CHA SCR catalyst. *React. Chem. Eng.* **2019**, *4*, 1067–1080. [[CrossRef](#)]
29. Fahami, A.R.; Günter, T.; Doronkin, D.E.; Casapu, M.; Zengel, D.; Vuong, T.H.; Simon, M.; Breher, F.; Kucherov, A.V.; Brückner, A.; et al. The dynamic nature of Cu sites in Cu-SSZ-13 and the origin of the seagull NO_x conversion profile during NH₃-SCR. *React. Chem. Eng.* **2019**, *4*, 1000–1018. [[CrossRef](#)]
30. Torregrosa-Rivero, V.; Albaladejo-Fuentes, V.; Sánchez-Adsuar, M.S.; Illán-Gómez, M.J. Copper doped BaMnO₃ perovskite catalysts for NO oxidation and NO₂-assisted diesel soot removal. *RSC Adv.* **2017**, *7*, 35228–35238. [[CrossRef](#)]
31. Wang, Z.; Lu, P.; Zhang, X.; Wang, L.; Li, Q.; Zhang, Z. NO_x storage and soot combustion over well-dispersed mesoporous mixed oxides via hydrotalcite-like precursors. *RSC Adv.* **2015**, *5*, 52743–52753. [[CrossRef](#)]
32. Zhao, H.; Zhou, X.; Wang, M.; Xie, Z.; Chen, H.; Shi, J. Highly active MnO_x-CeO₂ catalyst for diesel soot combustion. *RSC Adv.* **2017**, *7*, 3233–3239. [[CrossRef](#)]
33. Cheng, Y.; Song, W.; Liu, J.; Zhao, Z.; Wei, Y. Simultaneous removal of PM and NO_x over highly efficient 3DOM W/Ce_{0.8}Zr_{0.2}O₂ catalysts. *RSC Adv.* **2017**, *7*, 56509–56518. [[CrossRef](#)]
34. Andreoli, S.; Deorsola, F.A.; Galletti, C.; Pirone, R. Nanostructured MnO_x catalysts for low-temperature NO_x SCR. *Chem. Eng. J.* **2015**, *278*, 174–182. [[CrossRef](#)]
35. France, L.J.; Yang, Q.; Li, W.; Chen, Z.; Guang, J.; Guo, D.; Wang, L.; Li, X. Ceria modified FeMnO_x—Enhanced performance and sulphur resistance for low-temperature SCR of NO_x. *Appl. Catal. B Environ.* **2017**, *206*, 203–215. [[CrossRef](#)]
36. Lu, X.; Song, C.; Jia, S.; Tong, Z.; Tang, X.; Teng, Y. Low-temperature selective catalytic reduction of NO_x with NH₃ over cerium and manganese oxides supported on TiO₂-graphene. *Chem. Eng. J.* **2015**, *260*, 776–784. [[CrossRef](#)]
37. Sitshebo, S.; Tsolakis, A.; Theinnoi, K.; Rodríguez-Fernández, J.; Leung, P. Improving the low temperature NO_x reduction activity over a Ag-Al₂O₃ catalyst. *Chem. Eng. J.* **2010**, *158*, 402–410. [[CrossRef](#)]
38. Chen, P.; Rizzotto, V.; Xie, K.; Simon, U. Tracking mobile active sites and intermediates in NH₃-SCR over zeolite catalysts by impedance-based in situ spectroscopy. *React. Chem. Eng.* **2019**, *4*, 986–994. [[CrossRef](#)]
39. Herreros, J.M.; George, P.; Umar, M.; Tsolakis, A. Enhancing selective catalytic reduction of NO_x with alternative reactants/promoters. *Chem. Eng. J.* **2014**, *252*, 47–54. [[CrossRef](#)]
40. Guilhaume, N.; Bassou, B.; Bergeret, G.; Bianchi, D.; Bosselet, F.; Desmartin-Chomel, A.; Jouguet, B.; Mirodatos, C. In situ investigation of diesel soot combustion over an AgMnO_x catalyst. *Appl. Catal. B Environ.* **2012**, *119–120*, 287–296. [[CrossRef](#)]
41. Portet-Koltalo, F.; Machour, N. Analytical methodologies for the control of particle-phase polycyclic aromatic compounds from diesel engine exhaust. In *Diesel Engine-Combustion, Emissions and Condition Monitoring*; IntechOpen: Rijeka, Croatia, 2013.
42. Penetrante, B.M.; Brusasco, R.M.; Merritt, B.T.; Pitz, W.J.; Vogtlin, G.E.; Kung, M.C.; Kung, H.H.; Wan, C.Z.; Voss, K.E. Plasma-assisted catalytic reduction of NO_x. *SAE Trans.* **1998**, *107*, 1222–1231.
43. Hoard, J. *Plasma-Catalysis for Diesel Exhaust Treatment: Current STATE of the Art*; SAE International: New York, NY, USA, 2001.

44. Wang, Z.; Kuang, H.; Zhang, J.; Chu, L.; Ji, Y. Nitrogen oxide removal by non-thermal plasma for marine diesel engines. *RSC Adv.* **2019**, *9*, 5402–5416. [[CrossRef](#)]
45. Talebizadeh, P.; Babaie, M.; Brown, R.; Rahimzadeh, H.; Ristovski, Z.; Arai, M. The role of non-thermal plasma technique in NO_x treatment: A review. *Renew. Sustain. Energy Rev.* **2014**, *40*, 886–901. [[CrossRef](#)]
46. Zhang, L.; Sha, X.L.; Zhang, L.; He, H.b.; Ma, Z.h.; Wang, L.W.; Wang, Y.X.; She, L.X. Synergistic catalytic removal NO_x and the mechanism of plasma and hydrocarbon gas. *AIP Adv.* **2016**, *6*, 075015. [[CrossRef](#)]
47. Jo, J.-O.; Trinh, Q.H.; Kim, S.H.; Mok, Y.S. Plasma-catalytic decomposition of nitrous oxide over γ -alumina-supported metal oxides. *Catal. Today* **2018**, *310*, 42–48. [[CrossRef](#)]
48. Lee, J.B.; Kang, H.C.; Jo, O.J.; Mok, S.Y. Consideration of the role of plasma in a plasma-coupled selective catalytic reduction of nitrogen oxides with a hydrocarbon reducing agent. *Catalysis* **2017**, *7*, 325. [[CrossRef](#)]
49. Nguyen, D.B.; Heo, I.J.; Mok, Y.S. Enhanced performance at an early state of hydrocarbon selective catalyst reduction of NO_x by atmospheric pressure plasma. *J. Ind. Eng. Chem.* **2018**, *68*, 372–379. [[CrossRef](#)]
50. Nguyen, D.B.; Nguyen, V.T.; Heo, I.J.; Mok, Y.S. Removal of NO_x by selective catalytic reduction coupled with plasma under temperature fluctuation condition. *J. Ind. Eng. Chem.* **2019**, *72*, 400–407. [[CrossRef](#)]
51. Manley, T. The electric characteristics of the ozonator discharge. *Trans. Electrochem. Soc.* **1943**, *84*, 83–96. [[CrossRef](#)]
52. Nguyen, D.B.; Lee, W.G. Implementation of alternative gas compositions and effects on discharge properties of atmospheric pressure plasma in decomposition of CHF₃. *J. Ind. Eng. Chem.* **2017**, *52*, 7–11. [[CrossRef](#)]
53. Nguyen, D.B.; Lee, W.G. Analysis of helium addition for enhancement of reactivity between CH₄ and CO₂ in atmospheric pressure plasma. *J. Ind. Eng. Chem.* **2015**, *32*, 187–194. [[CrossRef](#)]
54. Nguyen, D.B.; Lee, W.G. Effects of self-heating in a dielectric barrier discharge reactor on CHF₃ decomposition. *Chem. Eng. J.* **2016**, *294*, 58–64. [[CrossRef](#)]
55. Nguyen, D.B.; Lee, W.G. Effects of ambient gas on cold atmospheric plasma discharge in the decomposition of trifluoromethane. *RSC Adv.* **2016**, *6*, 26505–26513. [[CrossRef](#)]
56. Andana, T.; Piumetti, M.; Bensaid, S.; Russo, N.; Fino, D.; Pirone, R. Chapter 16—Advances in cleaning mobile emissions: NO_x-assisted soot oxidation in light-duty diesel engine vehicle application. In *Horizons in Sustainable Industrial Chemistry and Catalysis*; Albonetti, S., Perathoner, S., Quadrelli, E.A., Eds.; Studies Surface Science Catalysis; Elsevier: Amsterdam, The Netherlands, 2019; pp. 329–352.
57. Luo, Y.R. *Comprehensive Handbook of Chemical Bond Energies*; CRC Press: Boca Raton, FL, USA, 2007.
58. Zhang, Z.S.; Crocker, M.; Chen, B.B.; Wang, X.K.; Bai, Z.F.; Shi, C. Non-thermal plasma-assisted NO_x storage and reduction over cobalt-containing LNT catalysts. *Catal. Today* **2015**, *258*, 386–395. [[CrossRef](#)]

